

A power control strategy to improve power system stability in the presence of wind farms using FACTS devices and predictive control



Mohsen Darabian*, Abolfazl Jalilvand

Department of Electrical Engineering, University of Zanjan, Zanjan, Iran

ARTICLE INFO

Article history:

Received 29 February 2016
Received in revised form 14 June 2016
Accepted 6 August 2016
Available online 24 August 2016

Keywords:

Power system stability
Predictive control
Static Synchronous Series Compensator (SSSC)
Super Capacitor Energy Storage System (SCESS)
Doubly Fed Induction Generator (DFIG)
Wind turbine

ABSTRACT

The main objective of this paper that distinguishes it from other similar articles is to employ predictive control strategy to improve the stability of power systems (4- machines and 10-machine) in presence of wind farms based on Doubly Fed Induction Generator (DFIG), using Static Synchronous Series Compensator (SSSC) and Super Capacitor Energy Storage System (SCESS). In this paper, SCESS is used to control the active power in the Grid Side Converter (GSC) and SSSC is employed to reduce low frequency oscillations. The proposed strategy based on the predictive control can be simultaneously used to control the active and reactive power of the Rotor Side Converter (RSC) as well as damping controller design for SCESS and SSSC. A function is used in the predictive control strategy to reduce computational complexity in selecting the input paths of Laguerre functions. Moreover, the sampling time is reduced by means of employing the exponential data weighting. Simulation results for the function-based predictive control using disturbance scenario in the field of non-linear time are compared with the other two methods, model-based predictive control and classic model (without using the predictive control). The effectiveness of the proposed strategy in improving stability is confirmed through simulation result.

© 2016 Elsevier Ltd. All rights reserved.

1. Introduction

1.1. Motivation and approach

Due to world population growth today, diminishing fossil fuels sources and concerns about environmental pollution, the use of renewable energy resources has drawn more and more attention of researchers. Among the renewable energy sources, wind energy is one of the most popular type of energy to produce electricity throughout the world. But because of the fluctuating nature of wind power, the use of this energy causes the electricity produced by wind farms to be oscillated in electrical grids. Hence, the existence of such fluctuations from the stability and power quality point of view is non-negligible in a power system [1,2]. This can be considered in all types of variable and constant speed wind turbines. In this regard, the use of Energy Storage System (ESS) and Flexible AC Transmission Systems (FACTS) devices can be very useful as a compensator to reduce oscillations and increase damping in power systems [3,4]. Extensive studies have been done in the field of power system stability in the presence of wind farms and compensator devices. However, finding a method that can lead to

the development of industry and technology requires previous studies and employing their advantages and disadvantages. Therefore, in this paper that its main objective is to use the predictive control strategy to improve the stability of a hybrid power system including wind farms, synchronous generators, energy storage systems and FACTS devices, the most recent studies in each field are needed to be evaluated.

1.2. Review of previous publications

Due to low-cost and direct control of active and reactive power, doubly fed induction generator is considered as one of the most common types of variable speed wind turbine [5]. The rotor of this generator is connected to the grid through a back-to-back bi-directional converter and its stator is connected directly to the grid. A three loop controller including GSC, RSC and a control loop for DC link capacitor for connecting these two converters is used to control the bi-directional converter. Several studies have been made in recent years to stabilize the DFIG control systems, some of which include sensitivity analysis [6], small signal stability analysis [6–8], eigenvalues analysis [9], approaches based on optimizing control parameters in each of DFIG converters [10–12], a state feedback [13] and robust control H_2/H_∞ [14]. In the optimization-based methods, the parameters of PI controller in

* Corresponding author.

E-mail addresses: M.Darabian@znu.ac.ir (M. Darabian), ajalilvand@znu.ac.ir (A. Jalilvand).

Nomenclature

$P_{\omega t}$	extracted power from the wind turbine (W)	C_{dc}	capacity of the DC link capacitor
$\rho_{\omega t}$	air density (kg/m^3)	V_{dc}	voltage of the DC link capacitor
$K_{\omega t}$	swept area of blades (m^2)	Z_{q1} & Z_{i1}	PI controller coefficients for regulating the reactive power
$V_{\omega t}$	wind speed (m/s);	Z_{q2} & Z_{i2}	voltage of the DC link capacitor
$D_{\omega t}$	performance coefficient of blades	Z_{q3} & Z_{i3}	PI controller coefficients for regulating the reactive power
$\beta_{\omega t}$	blade pitch angle	i_{drw_ref}	current control in d -axis for RSC
$\lambda_{\omega t}$	tip speed ratio	i_{qrw_ref}	current control in q -axis for RSC
$d_1 - d_9$	constants	Q_{sw_ref}	reference reactive power
R_b	blade radius (m)	ω_{rw_ref}	reference speed
ω_b	angular velocity of blade (rad/s)	Z_{bg} & Z_{ig}	coefficients of the PI controller for regulating the voltage of DC link capacitor
L_{ss}	self-inductance of stator	Z_{pb} & Z_{pi}	coefficients of the PI controller for regulating the current of GSC
L_{rr}	self-inductance of rotor	i_{qgw_ref}	reference current control in q -axis for GSC
L_{mm}	mutual inductance	V_{dc_ref}	reference voltage of the DC link capacitor
R_s	stator resistance	$Z_{b\beta}$ & $Z_{i\beta}$	coefficients of the PI controller
R_r	rotor resistance	$\tau_{b\beta}$	delay time constant for blade pitch angle control
i_{ds}	stator current in d -axis	P_{gw}	power of wind turbine measured for the blade pitch control
i_{qs}	stator current in q -axis	P_{gw_ref}	reference power of wind turbine for the blade pitch control
i_{dr}	rotor current in d -axis	$x(k)$	state vector of MPC
v_{ds}	rotor current in q -axis	$u(k)$	input vector of MPC
v_{dr}	stator voltage in d -axis	$e(k)$	disturbance vector of MPC
v_{qs}	stator voltage in q -axis	$y(k)$	output vector of MPC
v_{dr}	rotor voltage in d -axis	k	sampling instant
v_{qr}	rotor voltage in q -axis	G_k	weighting matrix of the cost function
H_t	inertia constant of wind turbine	S_k	weighting matrix of control action in the cost function
H_g	inertia constant of generator	$y'(n+k)$	prediction vector of the output signal
ω_t	angular speed of wind turbine	$y_{ref}(n+k)$	reference path of system's future
ω_r	angular speed of rotor of generator	$\Delta u(n+k)$	action control vector
$T_{\omega t}$	mechanical torque of wind turbine	m_c	turns ratio of the coupling transformer of SSSC
T_{tg}	shaft torque	Z_{inv}	modulation index of SSSC
$T_{e\omega t}$	electrical torque of wind turbine	V_{dc_sssc}	DC capacitor voltage of SSSC
K_t	damping coefficient of turbine	β_s	phase angle of the injected voltage of SSSC
K_g	damping coefficient of generator		
K_{tg}	inertia constant of wind turbine		
L_{tg}	inertia constant of generator		
P_{dc}	active power of the DC link		
P_{rw}	active power of the rotor-side converter		
P_{gw}	active power of the grid-side converter		

each of the induction generator converters are optimized by intelligent algorithms to apply the output of the controller with the lowest error to the relevant converter. PI controllers core problem is their dependence on operating point as well as their sensitivity to change in system conditions. Hence, the neural network and fuzzy logic based algorithms have been used in some studies to solve this problem which have their own complexity and disadvantages as well [15,16]. Another method for reducing oscillations of the DFIG output power is to use Super Capacitor Energy Storage System [17,18]. Given that the use of power electronic devices is reduced in energy storage systems, in addition to reducing the cost in case of designing a proper controller, an output power with the lowest oscillation will be achieved by DFIG [19]. In these systems, if the wind turbine undergoes oscillations as a result of drastic change in wind, the power required by the system can be easily compensated through a DC-DC converter [20]. In addition, Fly-wheel Energy Storage System (FESS) [21,22], and Superconducting Magnetic Energy Storage (SMES) can be noted as other energy storage systems used at AC bus to compensate reactive power [23–25]. One of the methods to reduce low frequency oscillation (LFO) in the power system stability studies is to design damping controller for power system stabilizer (PSS) or FACTS devices. The SSSC is a new generation of FACTS devices which is connected in series with transmission lines and leads the power flowing in transmission

lines to be converted from capacitive to inductive [26,27]. Therefore, the regional and inter-regional oscillations can be mitigated through a proper controller design for SSSC and PSS. Different methods have been proposed to design a suitable controller for SSSC [28–33]. Wavelet neural adaptive method to design PID controller [28], nonlinear robust control method to improve damping and transient stability [29], methods based on intelligent algorithms to optimize lead-lag controller parameters in the design of coordinated PSS-SSSC [30,31], damping controller design for SSSC in the presence of wind farms using adaptive-network-based fuzzy inference system (ANFIS) considering time delay [32] and modal analysis [33] are some of the approaches to increase stability of power systems using this type of FACTS devices. The above-mentioned techniques are able to provide a desired response to system in case of the detailed design. But in case of multiple disturbances in a power system and lack of certainty in a wind system, a method is required to guarantee stability under all conditions. In other words, this method should be able to apply the constraints of the system as well as simultaneously control of multiple parameters with the lowest output error so as to ensure the stability of the system. The predictive control is presented as a very powerful control tool for meeting the above requirements. Model Predictive Control (MPC) is assumed as one of the advanced control methods in the field of industrial operations and research

activities [34]. In this method, by employing the process model and minimizing an objective function, reasonable control signals are achieved to design the control loop parameters.

The selection of appropriate control signals for Power System Stabilizer (PSS) [35], the design of damping controller for a HVDC system [36], the control of active and reactive power in a wind turbine modeled in the state space [37,38], the control of active and reactive power in a micro-grid to coordinate wind turbine and a battery considering wind speed and network consumption [39] and the prediction of out power of a micro-grid to control voltage and active power in a 33-buses distribution system [40] are some of MPC applications in solving problems related to power system stability. Different predictive control strategies have been proposed in various references, all of which are based on the model predictive. It has been tried in these methods to employ some mathematical equations and intelligent algorithms to improve the process of solving the predictive model problems. In this regard, the non-linear predictive model with Offset-Free to design Static Var Compensator (SVC) [41], robust predictive control to design control signals of FACTS devices to improve transient stability [42], the non-linear predictive control based on Takagi–Sugeno

fuzzy model [43], distributed model predictive control [44] and functional predictive control [45,46] are included as more advanced methods for predictive model which are required to implement the advanced mathematical equations in the field of control engineering.

1.3. Contributions

In this paper, functional model predictive control is used to enhance stability of the four machine power system with approach of the active and reactive power control in a wind turbine. Active power control in grid-side convertor is carried out using a damping controller in the SCESS structure. This structure is designed in such a way that in addition to balancing DC voltage link, have the ability to control the active power in GSC. The active and reactive power control in the rotor-side converter is conducted with the approach of selecting the proper control signals for the RSC inverter. Moreover, in order to mitigate low frequency oscillations, a damping controller is used in the SCESS structure to control line power flow and increase the power system damping.

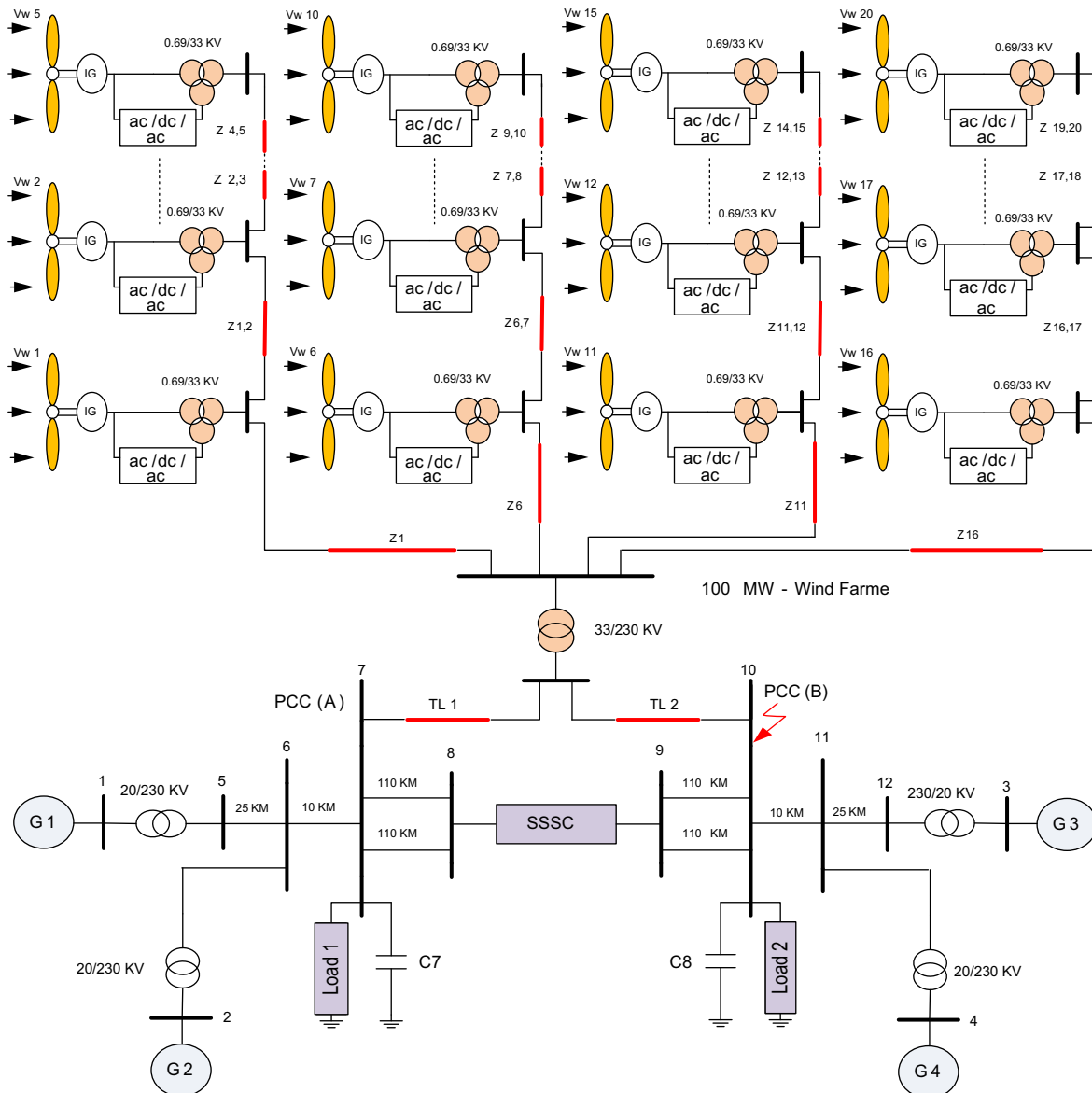


Fig. 1. The model of four-machine power system connected to the wind farm and SSSC-SCESS.

1.4. Paper structure

This paper is set out as follow: Section 2 presents the power system modeling including synchronous generator dynamic equations, the grid and rotor-side converters equations for DFIG and the damping controller design equations for SCESS and SSSC, Section 3 presents the modeling of predictive control strategy and its implementation on the power system, Section 4 presents the simulation results and finally the conclusion is presented in Section 5.

2. Modeling of power system elements

2.1. Synchronous generator model

In this section, the equations of the test system shown in Fig. 1 are described. In this paper, the two-axis model is employed to analyze the dynamic equations of the synchronous generator [47]. In the two-axis model, the impact of sub-transient reactance is ignored and only the synchronous generator transient reactance is used in the modeling. The excitation system including AVR-PSS is type IEEE-1 and its relevant parameters are given in Appendix A (Table 1). The two-axis model dynamic equations for the i_{th} synchronous generator can be stated as follow:

$$\frac{dE'_{qi}}{dt} = \frac{1}{T'_{doi}} [-E'_{qi} + E_{fdi} + (X_{di} - X'_{di})I_{di}] \quad (1)$$

$$\frac{dE'_{di}}{dt} = \frac{1}{T'_{qoi}} [-E'_{di} - (X_{qi} - X'_{qi})I_{qi}] \quad (2)$$

$$\frac{d\delta_i}{dt} = \omega_i - \omega_s \quad (3)$$

$$\frac{d\omega_i}{dt} = \frac{\omega_s}{2H_i} [T_{mi} - [I_{di}E'_{di} + I_{qi}E'_{qi} - (X'_{qi} - X'_{di})I_{di}I_{qi}] - D_i(\omega_i - \omega_s)] \quad (4)$$

2.2. Doubly fed induction generator model

In the DFIG based wind turbine system, the GSC and RSC are connected to each other through a DC link and in back-to-back form as seen in Fig. 2. The DC link duty is to keep the balance between two convertors. In this paper, the vector technique is used to model the synchronous generator to control the active and reactive powers [6]. But due to the space constraints, the electrical equations of synchronous generator, the mechanical and aerodynamic equations of wind turbine are ignored. But the equations of RSC and GSC controllers are fully expressed due to the control of active and reactive powers as the main subject of this paper. The more comprehensive information regarding the modeling of relevant controllers for DFIG is given in [6,9].

2.3. Mathematical model of RSC

The main duties of the RSC are to control the output active and reactive output power of DFIG, extract the maximum power from wind and provide the reactive power required by the induction generator. In this controller, active power and voltage are controlled by v_{qrw} and v_{drw} components, respectively. As seen in Fig. 3, voltage control is done through reactive power control by measuring Q_{sw} and reactive power control is carried out through measuring the turbine speed ω_{rw} . Comparing these control signals with reference signals by a PI controller for each of the parameters, the reference signals (i_{qrw_ref} , i_{drw_ref}) are produced. The reference signals in d-q axis are compared with the current reference signal to produce the error signal and then after passing through two PI controllers, v_{qrw}^* and v_{drw}^* signals are obtained. These reference signals after amplifying by two other components of current signals produce v_{qrw} , v_{drw} signals in order to be sent to PWM. And finally, a proper pulse is sent by PWM to the inverter to apply switching [9]. The RSC equations can be stated as follow:

Table 1
Employed system parameters.

Generator	G ₁	G ₂	G ₃	G ₄	Exciter	Exciter 1	Exciter 2	Exciter 3	Exciter 4
<i>Multi-machine power system</i>									
Rated MW	719	700	700	719	K_A	20	20	20	20
Rated MVAR	185	235	176	202	T_A (s)	0.2	0.2	0.2	0.2
Vbase kV	20	20	20	20	K_E	1	1	1	1
X_d (p.u.)	1.8	1.8	1.8	1.8	T_E (s)	0.314	0.314	0.314	0.314
X'_d (p.u.)	0.3	0.3	0.3	0.3	K_F	0.063	0.063	0.063	0.063
X_q (p.u.)	1.7	1.7	1.7	1.7	T_F (s)	0.35	0.35	0.35	0.35
X'_q (p.u.)	0.55	0.55	0.55	0.55	A_X	0.015	0.015	0.015	0.015
τ'_{do}	8	8	8	8	B_X	9.6	9.6	9.6	9.6
τ'_{qo}	0.05	0.05	0.05	0.05	-	-	-	-	-
H (s)	6.5	6.175	6.175	6.5	-	-	-	-	-
ω_s (p.u.)	1	1	1	1	-	-	-	-	-
<i>DFIG based wind turbine (100 MW)</i>									
$P = 5$ MW	$V = 0.69$ KV	$R_r = 0.042$ p.u.	$R_r = 0.005$ p.u.	$C_{dc} = 0.01$ F	$L_{mm} = 2.9$ p.u.	$L_{rr} = 3.056$ p.u.	$L_{ss} = 3.071$ p.u.		
$X_{lg} = 0.55$ p.u.	$K_t = 0.5$ p.u.	$K_{lg} = 2.5$ p.u.	$L_{lg} = 0.93$ p.u.	$H_t = 0.05$ p.u.	$H_g = 10.2$ p.u.	$Z_{q1} = 15$	$Z_{i1} = 9.2$		
$Z_{q2} = 8.6$	$Z_{i2} = 3.87$	$Z_{q3} = 15$	$Z_{i3} = 9.2$	$Z_{bg} = 17.35$	$Z_{ig} = 10.43$	$Z_{pb} = 12$	$Z_{ib} = 8.53$		
$\beta_{wt_min} = 0^\circ$	$\beta_{wt_max} = 30^\circ$	$Z_{p\beta} = 1.11$	$d_1 = 0.22$	$d_2 = 116$	$d_3 = 0.954$	$d_4 = 0.18$	$d_5 = 0.955$		
$d_6 = 6.161$	$d_7 = 11.89$	$d_8 = -12.95$	$d_9 = 0.088$	-	-	-	-		
<i>SSSC (± 50 MVAR)</i>									
$S = 50$ MVA	$V = 161$ kV	$F = 60$ HZ	$R = 0.01$	$L = 0.02$	$V_{dc} = 40$ kV	$C_{dc} = 175$ μ F	$Z_{b_sssc} = 0.0015$	$Z_{i_sssc} = 0.15$	
<i>Transmission lines</i>									
$R_{TL1} = R_{TL2} = 0.00005$ p.u.				$X_{TL1} = X_{TL2} = 0.0012$ p.u.					
$Z_1 = Z_6 = Z_{11} = Z_{16} = 0.0738 + j0.1050$ Ω				$Z_{1,2} = Z_{6,7} = Z_{11,12} = Z_{16,17} = 0.0771 + j0.1148$ Ω	$Z_{3,4} = Z_{8,9} = Z_{13,14} = Z_{18,19} = 0.2756 + j0.1558$ Ω				
$Z_{4,5} = Z_{9,10} = Z_{14,15} = Z_{19,20} = 0.3658 + j0.1591$ Ω				-					
<i>SCESS</i>									
$C = 20$ mF	$C_{ees} = 20$ F			$L_{ees} = 50$ mH			$V_{sc} = 2$ kV		$V_{dc} = 4$ kV

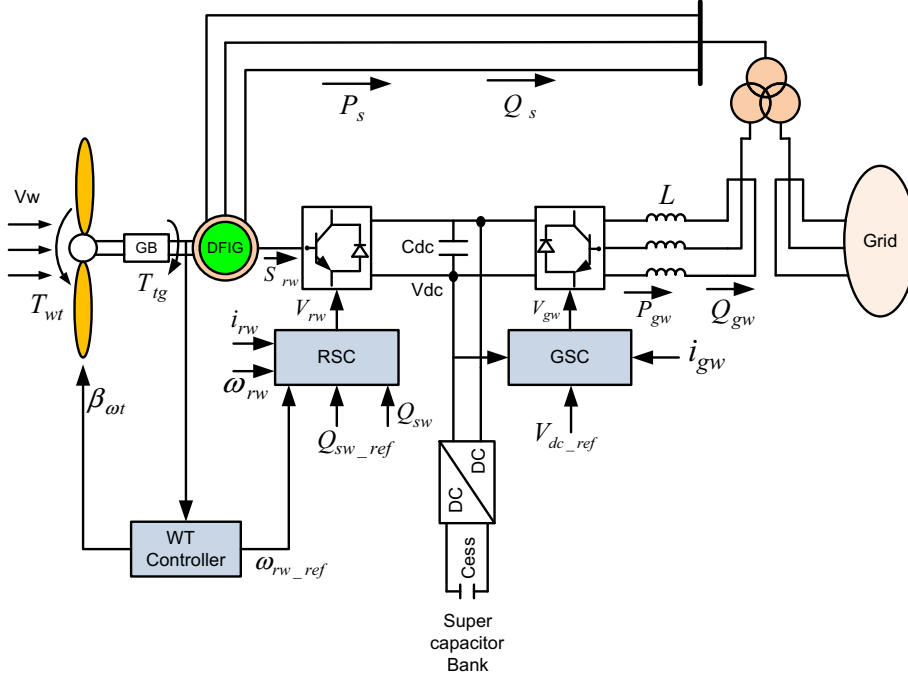


Fig. 2. Block diagram of DFIG-based wind turbine.

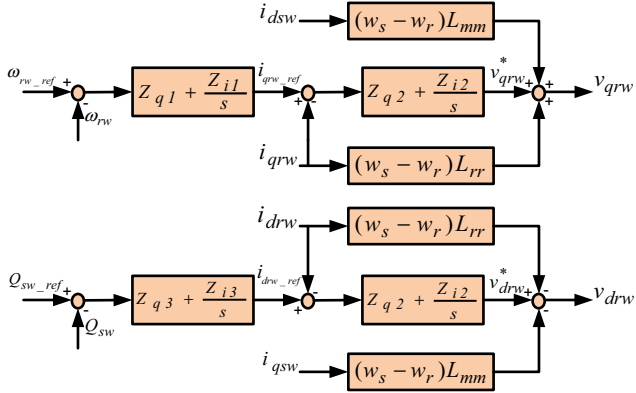


Fig. 3. Block diagram of the rotor-side converter.

$$\begin{cases}
 \dot{u}_1 = \omega_{rw_ref} - \omega_{rw} \\
 \dot{i}_{q_{rw_ref}} = Z_{q1}(\omega_{rw_ref} - \omega_{rw}) + Z_{i1}u_1 \\
 \dot{u}_2 = i_{q_{rw_ref}} - i_{q_{rw}} = Z_{q1}(\omega_{rw_ref} - \omega_{rw}) + Z_{i1}u_1 - i_{q_{rw}} \\
 \dot{u}_3 = Q_{sw_ref} - Q_{sw} \\
 \dot{i}_{d_{rw_ref}} = Z_{q3}(Q_{sw_ref} - Q_{sw}) + Z_{i3}u_3 \\
 \dot{u}_4 = i_{d_{rw_ref}} - i_{d_{rw}} = Z_{q3}(Q_{sw_ref} - Q_{sw}) + Z_{i3}u_3 - i_{d_{rw}} \\
 v_{q_{rw}} = Z_{q2}(Z_{q1}(\omega_{rw_ref} - \omega_{rw}) + Z_{i1}u_1 - i_{q_{rw}}) + Z_{i2}u_2 \\
 \quad + s_{rw}\omega_s L_{mm}i_{d_{sw}} + s_{rw}\omega_s L_{rr}i_{q_{rw}} \\
 v_{d_{rw}} = Z_{q2}(Z_{q3}(Q_{sw_ref} - Q_{sw}) + Z_{i3}u_3 - i_{d_{rw}}) \\
 \quad + Z_{i2}u_4 - s_{rw}\omega_s L_{mm}i_{q_{sw}} - s_{rw}\omega_s L_{rr}i_{d_{rw}}
 \end{cases} \quad (5)$$

2.4. Mathematical model of GSC

The main duties of the GSC are to keep the DC voltage Link in a constant value and control the reactive power of the network. The

detailed block diagram of the GSC is shown in Fig. 4. According to this figure, comparing the reference signal of DC link (v_{dc_ref}) with the measured value (v_{dc}) by a PI controller, the current reference signal in the d-axis is obtained. The current reference signals ($i_{q_{gw_ref}}$, $i_{d_{gw_ref}}$) are compared with the measured values and then after passing through two PI controllers, $v_{d_{gw}}^*$ and $v_{q_{gw}}^*$ signals are generated. This control signal after combining with the current signals generate $v_{q_{gw}}$, $v_{d_{gw}}$ signals in order to be sent to PWM. And finally, proper pulses provided by PWM are sent to the inverter to apply switching [9]. The GSC equations can be stated as follow:

$$\begin{cases}
 \dot{u}_5 = V_{dc_ref} - V_{dc} \\
 \dot{i}_{d_{gw_ref}} = -Z_{bg}\Delta V_{dc} + Z_{ig}u_5 \\
 \dot{u}_6 = i_{d_{gw_ref}} - i_{d_{gw}} = -Z_{bg}\Delta V_{dc} + Z_{ig}u_5 - i_{d_{gw}} \\
 \dot{u}_7 = v_{q_{gw_ref}} - i_{q_{gw}} \\
 \Delta v_{d_{gw}} = Z_{pg}u_6 + Z_{pi}u_6 = Z_{pg}(-Z_{bg}\Delta V_{dc} + Z_{ig}u_5 - i_{d_{gw}}) + Z_{pi}u_6 \\
 \Delta v_{q_{gw}} = Z_{pg}u_7 + Z_{pi}u_7 = Z_{pg}(i_{q_{gw_ref}} - i_{q_{gw}}) + Z_{pi}u_6
 \end{cases} \quad (6)$$

2.5. Controller of SCEES convertor

In this paper, a SCEES is used to guarantee the maintenance of the DC link voltage. In addition, a damping controller is designed in the SCEES system to control the reactive power of the system under network changes. This converter is composed of a capacitor bank and a dual switch DC/DC converter which is connected to the

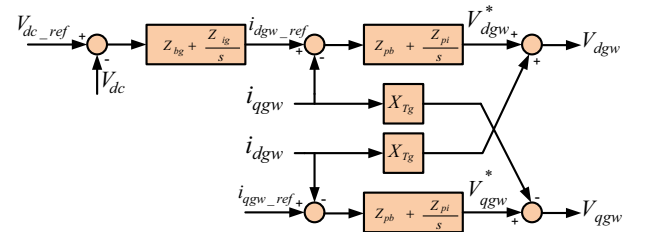


Fig. 4. Control block diagram of the grid-side converter.

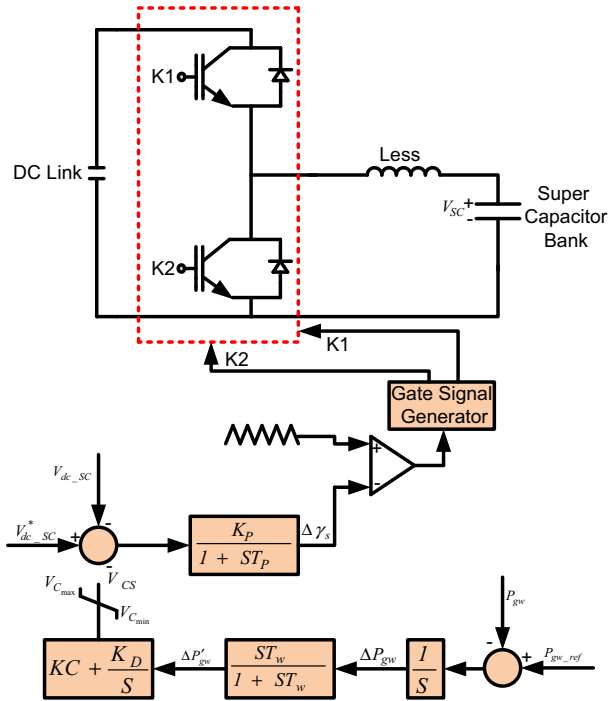


Fig. 5. Block diagram for designing the damping controller of the SCESS.

DFIG through the DC link (see Fig. 5). This converter can be used in boost and buck modes depending on the switches K_1 and K_2 . When K_1 is open, the converter operates in boost mode and in case of K_2 being open, the converter operates in buck mode. When K_1 is close (buck mode), based on the ratio of the capacitor bank voltage to the DC link voltage, the contribution of switch K_1 (when switch K_1 is on) can be obtained as follow (S_1):

$$S_1 = \frac{V_{sc}}{V_{dc}} \quad (7)$$

Moreover, when K_2 is close (boost mode), S_2 is defined as $1-S_1$. The ratio of the capacitor bank voltage to the DC link voltage is considered as 0.5 in this paper which means $S_1 = 0.5$. The SCEES equations can be formulated as follow:

$$\begin{cases} \frac{\Delta P'_{gw}}{dt} = P_{gw_ref} - P_{gw} \\ \frac{\Delta P'_{gw}}{dt} = (P_{gw_ref} - P_{gw}) - \frac{\Delta P'_{gw}}{T_w} \\ \frac{dV_{CS}}{dt} = K_C \left((P_{gw_ref} - P_{gw}) - \frac{\Delta P'_{gw}}{T_w} \right) + K_D \Delta P'_{gw} \\ \frac{d\Delta\gamma_s}{dt} = \frac{1}{T_p} [K_P (V_{dc_SC}^* - V_{dc_SC} - V_{CS}) - \Delta\gamma_s] \end{cases} \quad (8)$$

2.6. Mathematical model of SSSC

The SSSC can be used as a reactive power compensator based on voltage source inverter connected in series with transmission line. In other words, this compensator can operate in two modes: the capacitive and inductive. The structure of SSSC including a voltage source inverter, a series transformer, a capacitor of capacity C_{dc} and a control block is demonstrated in Fig. 6. The SSSC series injected voltage in d-q axis can be stated as follow using synchronous reference frame:

$$\begin{cases} v_{ds} = m_c Z_{inv} V_{dc_SSSC} \cos(\beta_s) \\ v_{qs} = m_c Z_{inv} V_{dc_SSSC} \sin(\beta_s) \end{cases} \quad (9)$$

Dynamic equation of DC link capacitor to preserve the balance of power in dc and ac sides is expressed as follow:

$$V_{dc_SSSC} = \frac{1}{C_{dc}} \left[m_c Z_{inv} (i_d \cos \beta_s + i_q \sin \beta_s) - \frac{V_{dc_SSSC}}{R_{dc}} \right] \quad (10)$$

The block diagram of SSSC for the capacitive mode along with damping controller is depicted in Fig. 7. By adding a control signal based on X_F , the transmitting power in the line can be controlled to reduce low frequency oscillations (see Fig. 7). The SSSC damping controller equations can be expressed as follows:

$$\begin{cases} \frac{\Delta P_L}{dt} = P_{L_ref} - P_L \\ \frac{\Delta P'_L}{dt} = (P_{L_ref} - P_L) - \frac{\Delta P'_L}{T_w} \\ \frac{dX_F}{dt} = K_F \left((P_{L_ref} - P_L) - \frac{\Delta P'_L}{T_w} \right) + K_A \Delta P'_L \end{cases} \quad (11)$$

3. Predictive control

In the problems requiring the prediction of system's future behavior, the model-based predictive control is a powerful technique [48,49]. The information predicted by this method is used to obtain the optimal point based on the criteria of each specific problem. As the basis of this method is on the process model, therefore, the predicted inputs and outputs can also be used for state estimation of the process. The new measurements of the process model sampled in each time instant are injected into the control loop, and on this basis, the predictive horizon is forecasted. The merit of this strategy is that in each sampling interval, a constrained optimization problem is solved. The limitations and every change in the process constraints can be applied to the system as the error signal. One of the appealing features of the predictive control which has distinguished it from the other control methods is that a series of control variables with a given length, i.e. the predictive horizon is calculated for the future behavior the system. Fig. 8 shows the block diagram of this control method. Based on

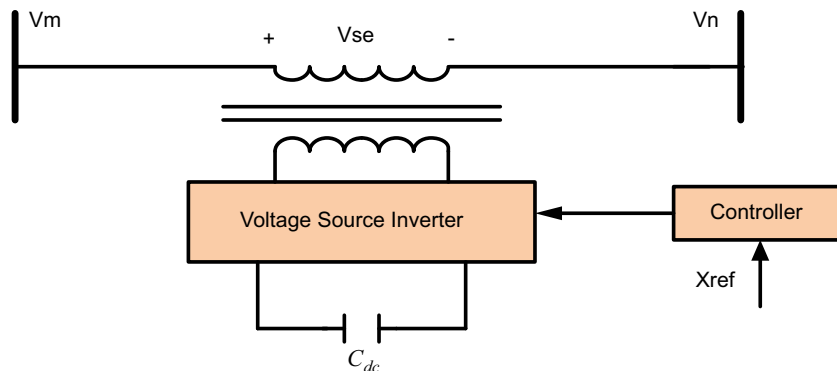


Fig. 6. Circuit structure of an SSSC.

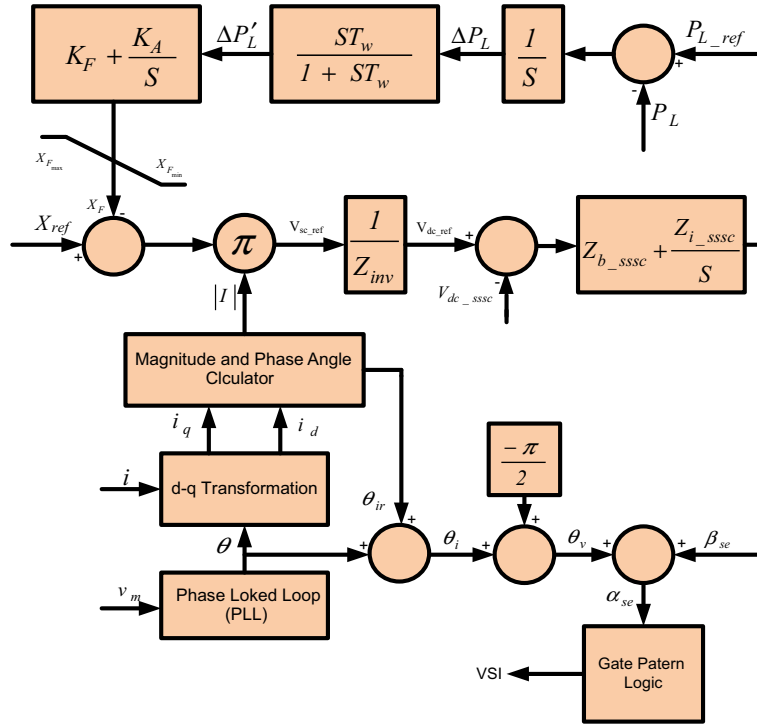


Fig. 7. Block diagram for designing the damping controller of the SSSC.

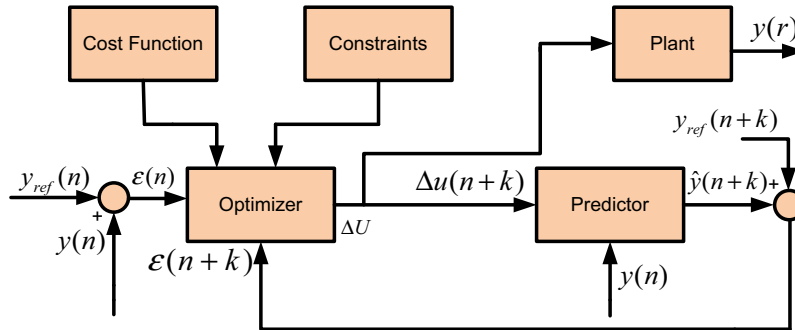


Fig. 8. Controller structure of the model predictive control.

this figure, the problem constraints, the objective function, and the output of the prediction system can be applied to the optimization system in order to obtain an appropriate output for the system. As in this paper the predictive control strategy in the multi-objective form is used, therefore, the utilized model is in the state space to accurately follow the desired objectives. Thus, the equations of the MPC are represented in the discrete state space as (12):

$$\begin{cases} x(k+1) = A_z x(k) + B_z u(k) + E_z d(k) \\ y(k) = C_z x(k) \end{cases} \quad (12)$$

The objective function is selected in a way that the future outputs are able to track the reference signal in the prediction horizon, and the required control action is low as possible as more. Therefore, in order to attain the desired objectives, the objective function of the predictive control can be described as (13):

$$F_{fit}(n) = \sum_{k=1}^{m_a} G_k (y'(n+k) - y_{ref}(n+k))^2 + \sum_{k=1}^{m_b} S_k \Delta u(n+k)^2 \quad (13)$$

According to the above relation, the prediction vector, which is considered for the system's output, is defined as a $1 \times m_a$ matrix in which m_a is called the prediction horizon; Also, Δu is a $1 \times m_b$ matrix in which m_b is named the control horizon.

3.1. The considered constraints in the model predictive control

The following constraints are considered in solving of the problem by the predictive control:

- Limitation on the amplitude and variations of the input;
- Limitation on the state variables;
- Limitation on the output variables.

The above constraints can be mathematically described as (14):

$$\begin{cases} u_{\min} \leq u(n+k) \leq u_{\max}, \Delta u_{\min} \leq \Delta u(n+k) \leq \Delta u_{\max} \\ x_{\min} \leq x(n+k) \leq x_{\max}, \Delta x_{\min} \leq \Delta x(n+k) \leq \Delta x_{\max} \\ y_{\min} \leq y(n+k) \leq y_{\max}, \Delta y_{\min} \leq \Delta y(n+k) \leq \Delta y_{\max} \end{cases} \quad (14)$$

The optimal input control sequence is given by solving the objective function (13) with system constraint (14).

3.2. Functional model predictive control (FMPC)

3.2.1. Laguerre-based model predictive control

In the conventional MPC, the future control signal is considered as a vector of forward shift operator with length of m_b .

$$\Delta U = [\Delta u(n), \dots, \Delta b(n+k), \dots, \Delta b(n+m_b-1)] \quad (15)$$

where m_b unknown control variables are achieved in the optimization procedure. If the controlled system is a multivariable system, then this procedure should be done for all inputs, which need large computational burden. Therefore, MPC may not be fast enough to be used as a real-time optimal control for such systems. The problem will be worse when large prediction horizon is needed to achieve high closed-loop performance. A solution to this drawback is using functional MPC. In the functional MPC, future input is assumed to be a linear combination of a few simple base functions. In principle, these could be any appropriate functions. However in practice, a polynomial basis is usually used [50]. This approximation of input trajectory can be more accurate by proper selection of base function. Using FMPC, the term used in the optimization procedure can be reduced to a fraction of that required by classical MPC. Therefore, the computational load will be reduced largely.

In this paper, orthonormal basis Laguerre function is used for modeling input trajectory. Laguerre polynomial is one of the most popular orthonormal base functions, which has extensive applications in system identification [51]. The z-transform of g-th Laguerre function is given by (16):

$$\Gamma_g = \frac{\sqrt{1-b^2}}{z-b} \left(\frac{z^{-1}-b}{1-bz^{-1}} \right)^{g-1}, 0 \leq b \leq 1 \quad (16)$$

In this transform, b is the pole of the power system; if $0 < b < 1$, the system will be stable.

Now, each input control signal can be described using the Laguerre functions as below:

$$\Delta u(n+k) \approx \sum_{g=1}^m a_g \cdot f_g(k) \quad (17)$$

In the above relation, f_g is the transposed form of the Laguerre functions defined in Eq. (16), and a_g is named the parameter vector. In practical applications, the value of m is considered to be lower than 10. Choosing larger values for m will increase the input paths prediction for the Laguerre functions.

3.2.2. Exponentially weighted model predictive control

Closed-loop performance of MPC depends on the magnitude of prediction horizon m_a . Generally, by increasing the magnitude of prediction horizon, the closed-loop performance will be improved. However, practically, selection of large prediction horizon is limited by numerical issue, particularly in the process with high sampling rate. One approach to overcome this drawback is to use exponential data weighting in model predictive control [52].

To design discrete model predictive control with exponential data weighting, input, state, and output vectors are changed in the following way (18):

$$\begin{cases} \Delta \hat{U}^T = [\rho^{-0} \Delta u(n), \dots, \rho^{-(m_b-1)} \Delta u(n+m_b-1)] \\ \hat{X}^T = [\rho^{-1} x(n+1), \dots, \rho^{-m_a} x(n+m_a)] \\ \hat{Y}^T = [\rho^{-1} y(n+1), \dots, \rho^{-m_a} y(n+m_a)] \end{cases} \quad (18)$$

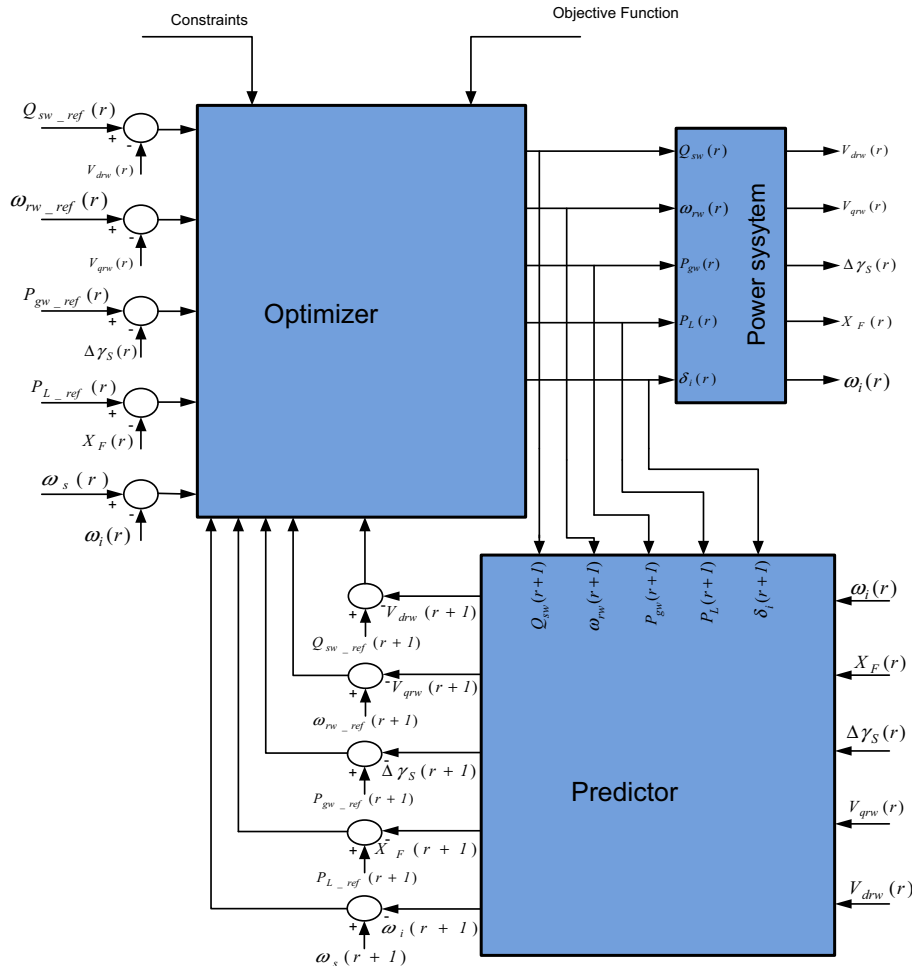


Fig. 9. Block diagram of the proposed strategy.

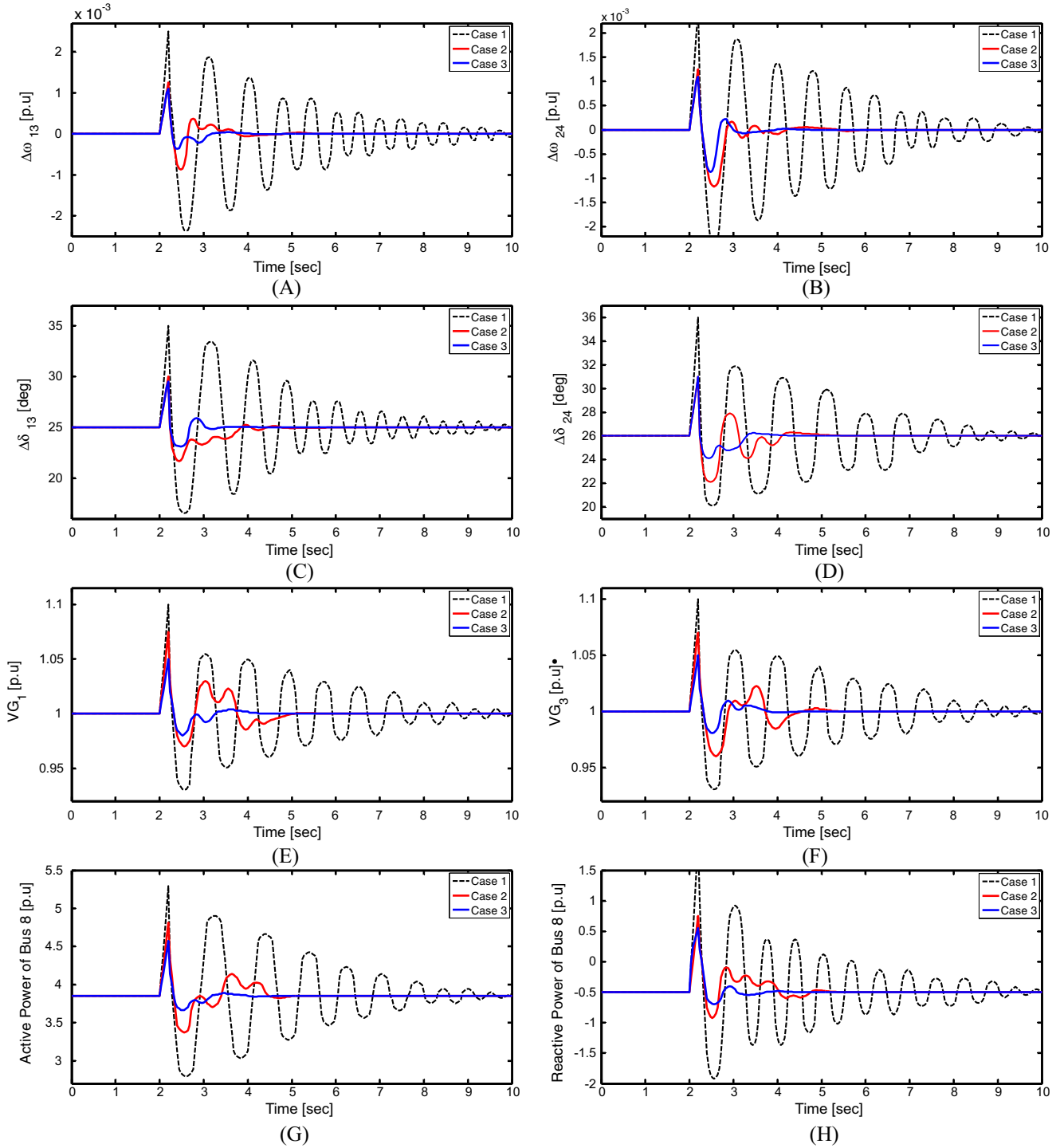


Fig. 10. The response of time-domain simulation of three-phase short circuit fault in four-machine power system.

In the above equation, the symbol ρ has been used for representing the adjustment of parameters in exponential weight. The value of ρ is chosen to be larger than 1. Therefore, the new equations of the utilized model in the state space can be explained as (19):

$$\begin{cases} \hat{x}(n+1) = \hat{A}\hat{x}(n) + \hat{B}\hat{\Delta}u(n) \\ \hat{y}(n) = \hat{C}\hat{x}(n) \end{cases} \quad (19)$$

Substituting the following relations in the above equation results in the new objective function of (21):

$$\hat{A} = \frac{A}{\rho}, \hat{B} = \frac{B}{\rho}, \hat{C} = \frac{C}{\rho} \quad (20)$$

$$\hat{F}_{fit}(n) = \sum_{k=1}^{m_a} G_k (\hat{y}(n+k) - k_{ref}(n+k))^2 + \sum_{k=1}^{m_b} S_k \hat{\Delta}u(n+k)^2 \quad (21)$$

Also, the constraints of (14) are modified to (22):

$$\begin{cases} \rho^{-z} u_{\min} \leq \hat{u}(n+k) \leq \rho^{-z} u_{\max}, \rho^{-z} \Delta u_{\min} \leq \hat{\Delta}u(n+k) \leq \rho^{-z} \Delta u_{\max} \\ \rho^{-z} x_{\min} \leq \hat{x}(n+k) \leq \rho^{-z} x_{\max}, \rho^{-z} \Delta x_{\min} \leq \hat{\Delta}x(n+k) \leq \rho^{-z} \Delta x_{\max} \\ \rho^{-z} y_{\min} \leq \hat{k}(n+k) \leq \rho^{-z} y_{\max}, \rho^{-z} \Delta y_{\min} \leq \rho^{-z} \Delta \hat{y}(n+k) \leq \rho^{-z} \Delta y_{\max} \end{cases} \quad (22)$$

After solving Eq. (21), the input path should be rewritten as (23):

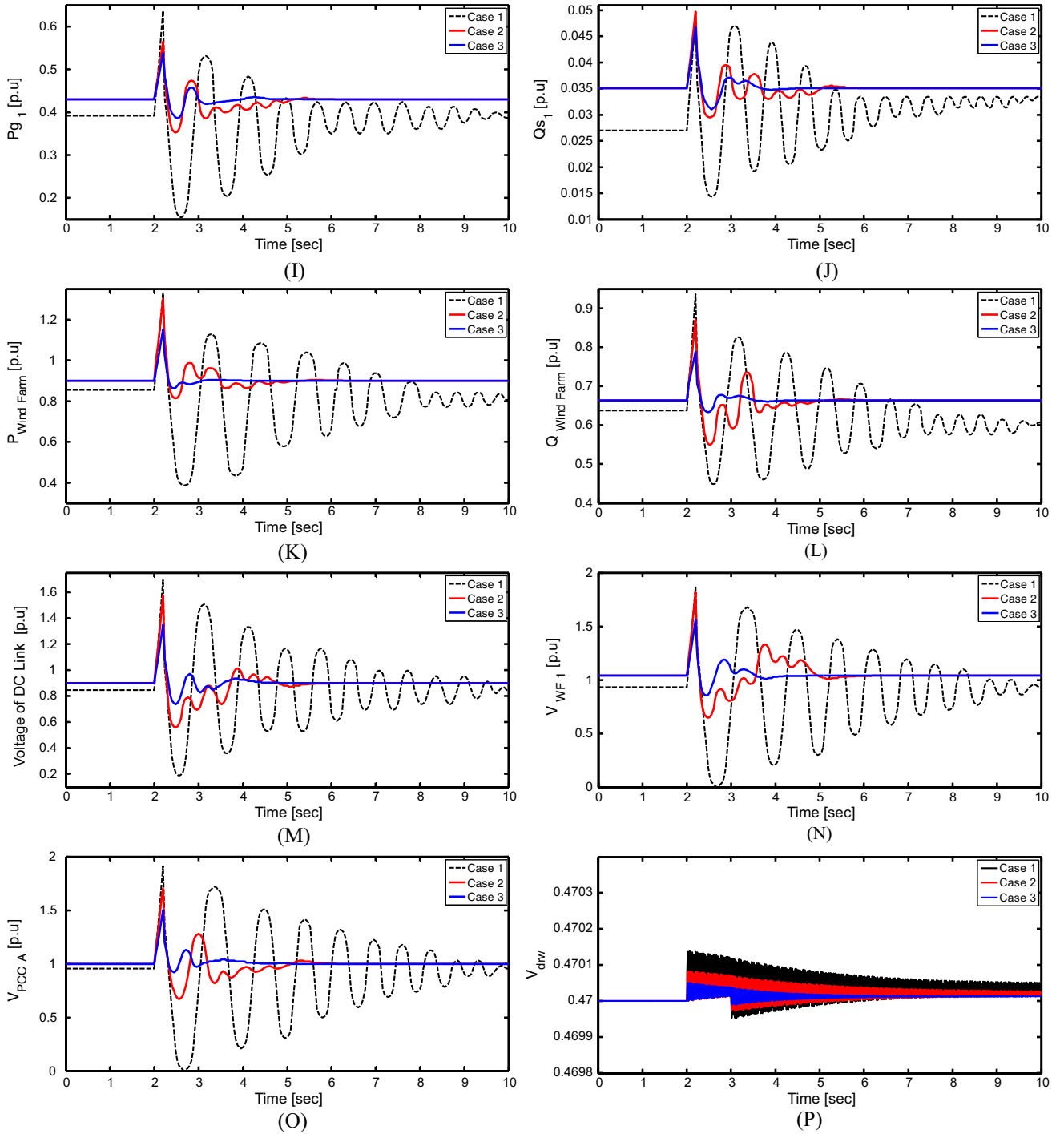


Fig. 10 (continued)

$$\Delta U^T = [b^0 \Delta \hat{u}(k), \dots, b^{(m_b-1)} \Delta \hat{u}(k + m_b - 1)] \quad (23)$$

In brief, the sequence of solving the problem of functional predictive control can be followed as the below stages:

- Assigning a proper value for ρ ;
- Substituting the matrices (A, B, C) and the variables (U, X, Y) in Eqs. (20) and (21);
- Applying the constraints in the objective function according to the characteristics of the problem using Eqs. (22) and (23);
- Implementing the optimization procedure for the objective function based on the Laguerre functions, and calculating the coefficients of this function;

- Processing the input control signals chosen by the Laguerre functions using Eq. (17).
- Sorting the inputs according to (23), and applying it to the considered system.

The functional MPC differs from the classical MPC in some cases; The Laguerre function and the exponentially weights represented in (16) and (17) are employed to produce the initial control input sequence $\Delta \hat{u}(n+k)$ in case of functional MPC. Then, by minimizing the cost function $\hat{F}_{fit}(n)$ described by (21) the optimal control trajectory is achieved by means of the initial control input sequence. The computational burden to acquire the optimal

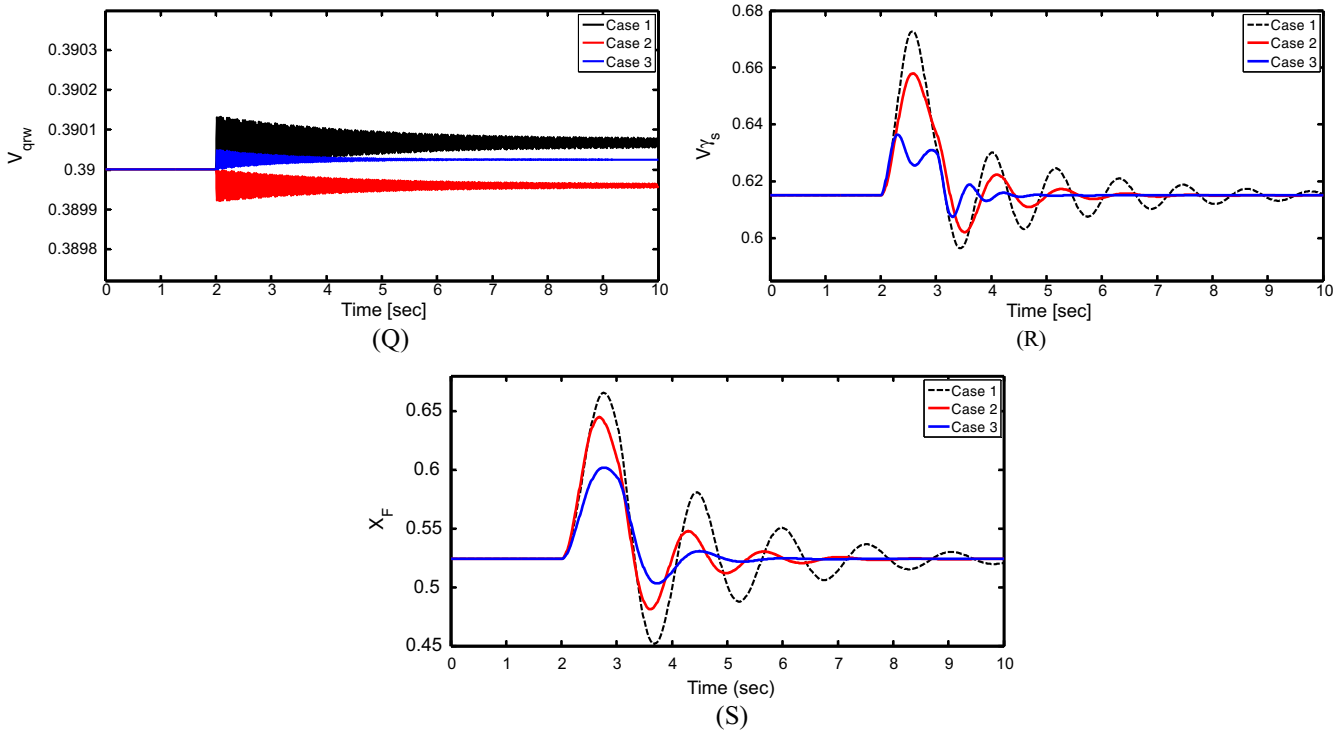


Fig. 10 (continued)

control trajectory is reduced employing the initial control input sequence with suitable weighting factors, G_k and S_k . Whereas, in case of classical MPC, minimizing the cost function $F_{fit}(n)$ described in (13) results in the optimal trajectory $\Delta u(n+k)$ directly. In order to minimize the cost function $F_{fit}(n)$ in this case, more calculations are required to obtain the optimal control trajectory.

3.3. Implementation of the proposed strategy for the system under study

In order to implement the predictive strategy on the system under study, the relations outlined in the strategy should be adapted to the power system model (as seen in Fig. 9). Therefore, it is essential to specify the network dynamic equations including synchronous generators, wind farm, SSSC and SCESS in state space. The state space equations can be represented as follow:

$$\begin{cases} \dot{X} = AX + BU + ER \\ Y = CX + DU \end{cases} \quad (24)$$

where X is the system state vector and is defined in this paper as follow:

$$\begin{cases} X = [X_{SG}, X_{RSC}, X_{GSC}, X_{SCESS}, X_{SSSC}]^T, \\ X_{SG} = [E'_{qi}, E'_{di}, \delta_i, \omega_i], X_{RSC} = [u_1, u_2, u_3, u_4] \\ X_{GSC} = [u_5, u_6, u_7], X_{SCESS} = [\Delta P'_{gw}, \Delta P'_{gw}, V_{CS}, \Delta \gamma_s], \\ X_{SSSC} = [\Delta P_L, \Delta P'_L, X_F] \end{cases}$$

where D is the variable value ($D=0$), U is the input vector of predictive control ($U = [\delta_i, \omega_{rw_ref}, Q_{sw_ref}, P_{gw_ref}, P_{L_ref}]^T$) and R is the disturbance vector ($R=0$). In order to modify the optimum response obtained from the predictive control, constraints should be defined within a legal range. In this paper, the constraints are defined as follow to achieve the desired objectives:

- Active and reactive powers control of DFIG with the approach of selecting proper reference vectors for the RSC ($V_{drw_min} \leq V_{drw} \leq V_{drw_max}$, $V_{qrw_min} \leq V_{qrw} \leq V_{qrw_max}$).

- Active power control of GSC with the approach of selecting proper output for damping controller in super capacitor energy storage system ($V_{\gamma s_min} \leq V_{\gamma s} \leq V_{\gamma s_max}$).
- Line power flow control with the approach of selecting proper output for damping controller in SSSC ($X_{F_min} \leq X_F \leq X_{F_max}$).

In general, the min/max ranges of the above-mentioned definitions are expressed as follow (25):

$$\begin{bmatrix} v_{drw_min} \\ v_{qrw_min} \\ V_{\gamma s_min} \\ X_{F_min} \\ \omega_{i_min} \end{bmatrix} = 0 \leq u \leq 1 = \begin{bmatrix} v_{drw_max} \\ v_{qrw_max} \\ V_{\gamma s_max} \\ X_{F_max} \\ \omega_{i_max} \end{bmatrix} \quad (25)$$

The constraints applied to control signals slow down the simulation speed whereas this problem does not happen in case of state vectors. Hence, the constraints applied to state vectors within a legal min/max range are stated as follow (26):

$$\begin{bmatrix} E'_{qi_min} \\ E'_{di_min} \\ u_{3_min} \\ u_{5_min} \end{bmatrix} = \begin{bmatrix} 0 \\ 0 \\ 0 \\ 0 \end{bmatrix} \leq x \leq \begin{bmatrix} 0.3 \\ 0.2 \\ 0.7 \\ 0.4 \end{bmatrix} = \begin{bmatrix} E'_{di_max} \\ E'_{di_max} \\ u_{3_max} \\ u_{5_max} \end{bmatrix} \quad (26)$$

In addition, the predictive control strategy parameters used in the simulation are set as $b=0.24$, $m=7$, $\rho=1.08$, $m_a=200$, $m_b=5$ for FMPC and $m_b=80$ for MPC. The coefficients in weight matrixes are selected as $G=0.14 \times I_{mb \times mb}$ and $S=1 \times I_{ma \times ma}$, respectively as well. The sampling time for the predictive controller is assumed as 0.03 s.

4. Simulation result

4.1. Four-machine two-area power system

As a larger system, a two area four machine power system equipped with a wind farm and a SSSC is employed to evaluate

Table 2
The eigen values of four-machine power system (in rad/s).

Operation points	Variables	PI	MPC	FMPC
$\omega_{r1...5} = 1.09$ p.u.	$\Delta\omega_{13}$	$-0.43 \pm 2.92j$	$-1.18 \pm 1.98j$	$-1.32 \pm 1.97j$
$V\omega_{1...5} = 12$ m/s	$\Delta\delta_{24}$	$-0.31 \pm 3.12j$	$-1.19 \pm 1.99j$	$-1.41 \pm 1.98j$
$\omega_{r6...10} = 1.03$ p.u.	V_{G3}	$-0.47 \pm 3.25j$	$-1.16 \pm 2.19j$	-1.46 ± 2.19
$V\omega_{6...10} = 11.5$ m/s	P_{Bus-8}	$-0.33 \pm 2.94j$	$-1.31 \pm 2.32j$	$-1.65 \pm 2.34j$
$\omega_{r11...15} = 1$ p.u.	Q_{Bus-8}	$-0.44 \pm 2.89j$	$-1.22 \pm 2.14j$	$-1.68 \pm 2.16j$
$V\omega_{11...15} = 11$ m/s	P_{g1}	$-0.38 \pm 2.99j$	$-1.35 \pm 2.17j$	$-1.75 \pm 2.17j$
$\omega_{r16...20} = 0.994$ p.u.	V_{WT-1}	$-0.31 \pm 3.09j$	$-1.21 \pm 2.15j$	$-1.54 \pm 2.14j$
$V\omega_{16...20} = 10.5$ m/s	Q_{WT-3}	$-0.48 \pm 3.31j$	$-1.27 \pm 2.23j$	$-1.68 \pm 2.23j$
$\omega_{r1...5} = 0.810$ p.u.	$\Delta\omega_{12}$	$-0.48 \pm 2.89j$	$-1.31 \pm 2.22j$	$-1.54 \pm 2.25j$
$V\omega_{1...5} = 8.5$ m/s	$\Delta\delta_{13}$	$-0.23 \pm 3.03j$	$-1.41 \pm 2.19j$	$-1.78 \pm 2.19j$
$\omega_{r6...10} = 0.925$ p.u.	V_{G4}	$-0.31 \pm 3.23j$	$-1.38 \pm 2.16j$	$-1.52 \pm 2.17j$
$V\omega_{6...10} = 9.5$ m/s	P_{Bus-8}	$-0.39 \pm 3.17j$	$-1.44 \pm 2.14j$	$-1.79 \pm 2.14j$
$\omega_{r11...15} = 1$ p.u.	Q_{Bus-8}	$-0.26 \pm 3.14j$	$-1.27 \pm 2.11j$	$-1.69 \pm 2.11j$
$V\omega_{11...15} = 11$ m/s	P_{g6}	$-0.13 \pm 3.54j$	$-1.49 \pm 2.26j$	$-1.96 \pm 2.25j$
$\omega_{r16...20} = 1.09$ p.u.	V_{WT-6}	$-0.18 \pm 3.87j$	$-1.53 \pm 2.31j$	$-2.04 \pm 2.29j$
$V\omega_{16...20} = 12$ m/s	Q_{WT-9}	$0.16 \pm 3.65j$	$-1.48 \pm 2.37j$	$-1.93 \pm 2.36j$
$\omega_{r1...5} = 0.729$ p.u.	$\Delta\omega_{34}$	$-0.36 \pm 3.96j$	$-1.16 \pm 1.95j$	$-1.59 \pm 1.96j$
$V\omega_{1...5} = 8$ m/s	V_{G3}	$-0.31 \pm 3.73j$	$-1.11 \pm 1.97j$	$-1.61 \pm 1.97j$
$\omega_{r6...10} = 0.875$ p.u.	P_{Bus-8}	$-0.28 \pm 4.76j$	$-1.27 \pm 2.21j$	$-1.85 \pm 2.23j$
$V\omega_{6...10} = 9$ m/s	Q_{Bus-8}	$-0.12 \pm 5.87j$	$-1.17 \pm 2.41j$	$-1.87 \pm 2.38j$
$\omega_{r11...15} = 0.975$ p.u.	P_{g11}	$-0.08 \pm 5.76j$	$-1.09 \pm 2.01j$	$-1.54 \pm 2.02j$
$V\omega_{11...15} = 10$ m/s	P_{g17}	$-0.03 \pm 5.98j$	$-1.15 \pm 2.12j$	$-1.78 \pm 2.12j$
$\omega_{r16...20} = 1$ p.u.	Q_{WT-12}	$-0.02 \pm 6.11j$	$-1.18 \pm 2.23j$	$-1.76 \pm 2.24j$
$V\omega_{16...20} = 11$ m/s	Q_{WT-17}	$-0.05 \pm 5.87j$	$-1.10 \pm 2.11j$	$-1.44 \pm 2.11j$

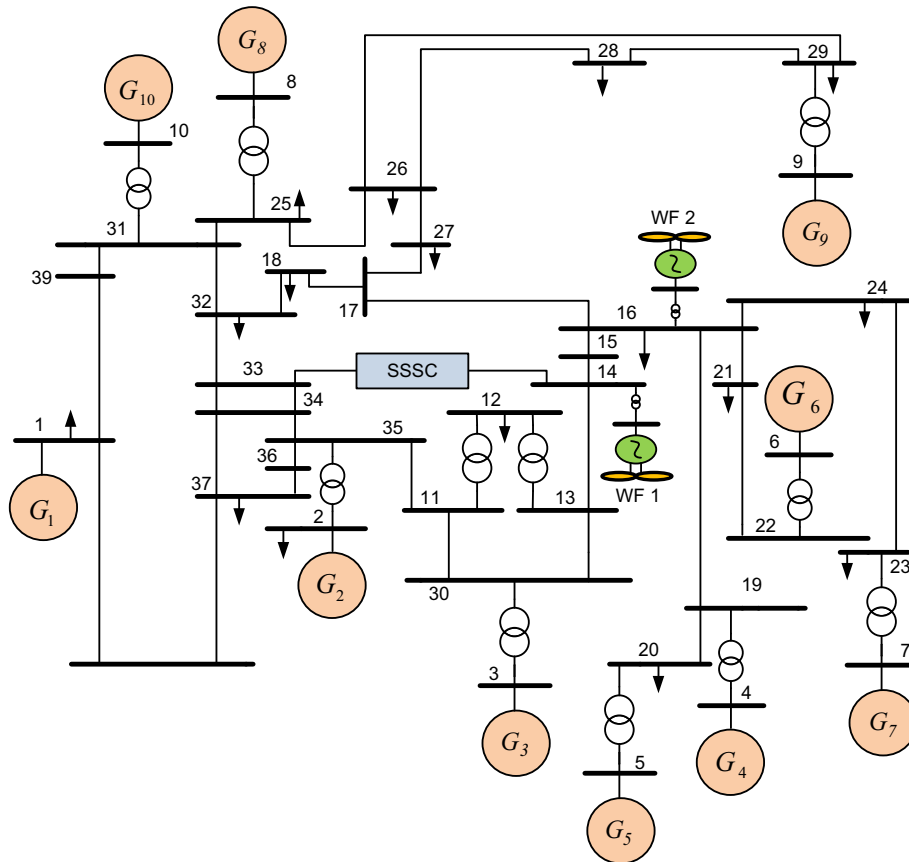


Fig. 11. Single-line diagram of New-England system with wind turbines and SSSC.

the proposed scheme. The wind farm consists of 20 wind turbines based on DFIG with capacity of 5 MW for each unit which is transferred through a 0.69/33 kV HV transformer. The total power produced by these turbines is 100 MW and is transferred to the power

system through a 33/230 kV HV transformer. It is worth mentioning that each of these turbines are equipped with SCESS and wind speed is considered as of 12 m per second for each of them. As seen in Fig. 1, a SSSC is used between buses 8 and 9 to

mitigate low frequency oscillation between two areas. The more detailed data of the system is given in Appendix A. A three-phase fault at $t=2\text{ s}$ is applied to Bus number 10 and cleared after 0.2 s.

Three different scenarios are considered as follow and results are shown in Fig. 10(A)–(I):

- Case1: PI controller in absence of SCESS-SSSC compensators.
- Case2: MPC controller in presence of SCESS-SSSC compensators.
- Case3: FMPC controller in presence of SCESS-SSSC compensators.

The variations in speed deviation for G_{1-3} and G_{2-4} are shown in Fig. 10(A) and (B), respectively. In addition, the variations in rotor

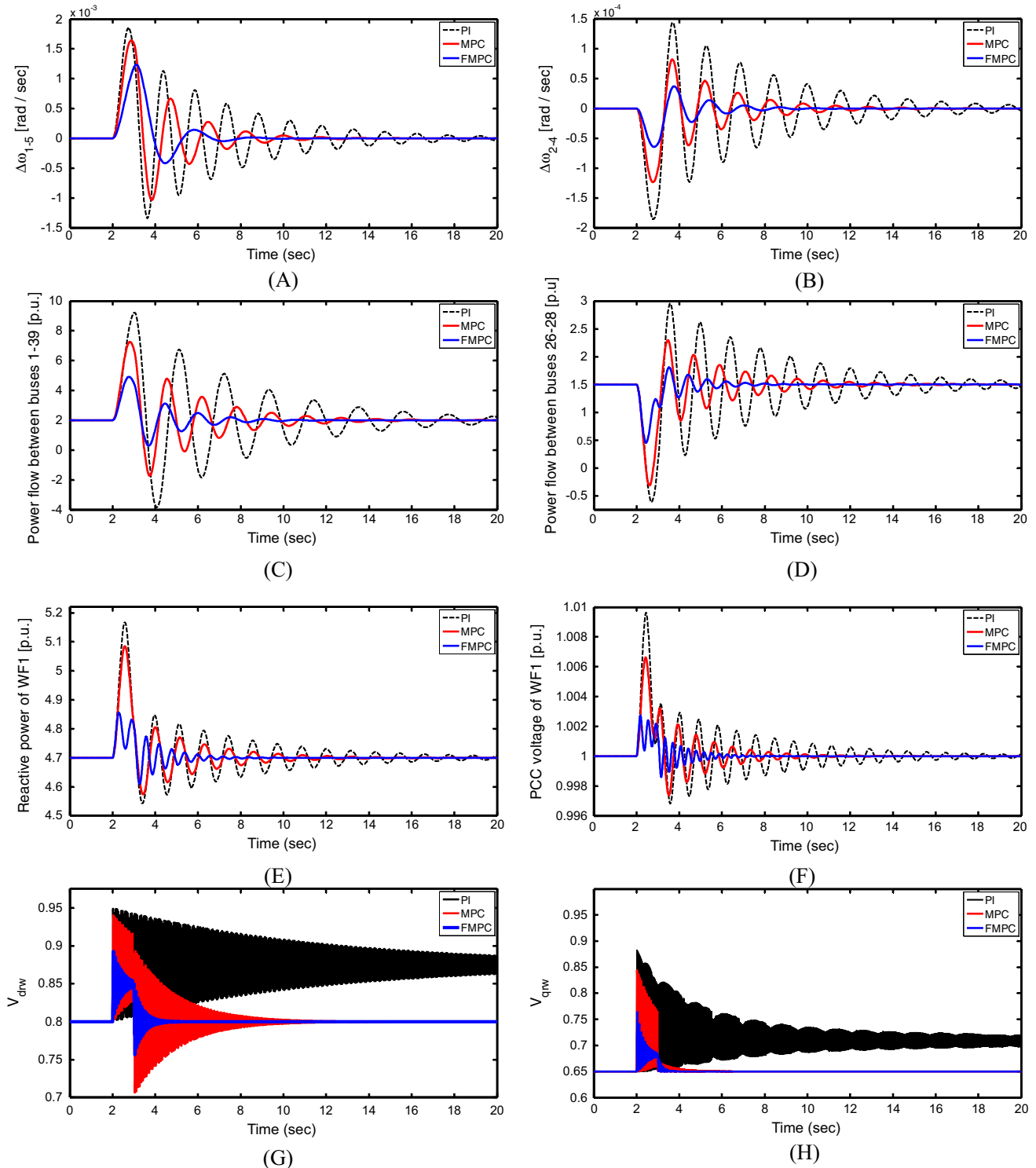


Fig. 12. The response of time-domain simulation of scenario I.

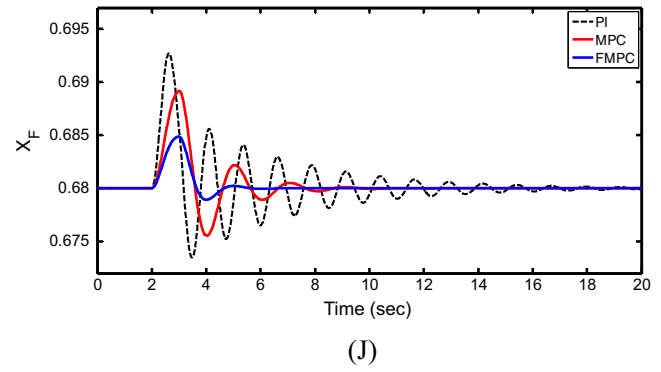
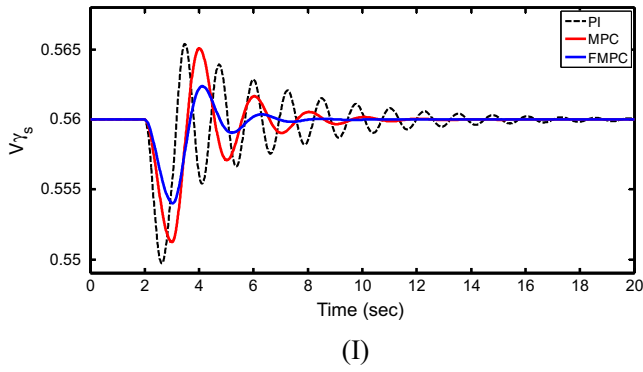


Fig. 12 (continued)

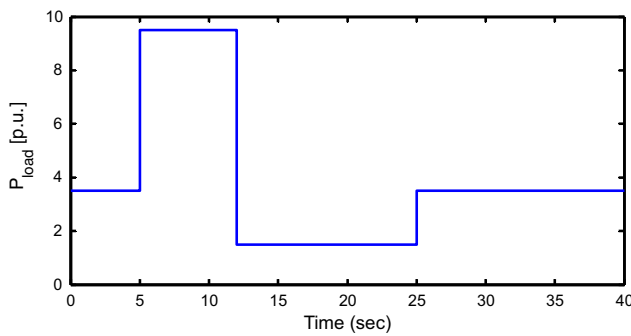


Fig. 13. The response of the load changes.

angle for G_{1-3} and G_{2-4} are depicted in Fig. 10(C) and (D), respectively. The better damping characteristics can be seen in the third case 3 compared to two other Cases. The terminal voltage of G1 and G3 are demonstrated in Fig. 10(E) and (F), respectively. As observed in these figures, the FMPC scheme is not only very successful in designing the damping controller, but also has significant impact on improving the dynamic stability of the power system. The variations in active and reactive power flown from bus 8 are shown in Fig. 10(G) and (H), respectively. The results of active power control (P_{gi}) on the GSC and reactive power control (Q_{Si}) on the RSC for wind turbine 1 are shown in Fig. 10(I) and (J), respectively. The responses of whole wind farm active and reactive power are illustrated in Fig.10(K) and (L). According to these figures, better performance by the wind farm and consequently better improvement in the power system stability are acquired through designing the damping controller for SSSC. The response of the DC link voltage and the terminal voltage for wind turbine 1 are shown in Fig.10(M) and (N), respectively. Moreover, Fig. 10 (O) illustrates the response of voltage variations for bus PCC (A). Fig. 10(P) and (Q) respectively show rotor-side converter switching signals on axis d and q. Furthermore, the input damping signals for SCESS and SSSC through the predictive controllers and PI controller are illustrated in Fig. 10(R) and (S), respectively.

Based on these figures, the average settling time for Cases 1–3 is reached as 9.963, 5.221 and 3.171 s, respectively. Also, the simulation time of the FMPC, MPC, and PI controller is 768.246, 892.324 and 741.987 s, respectively. Thus, it can be said that the functional model predictive controller is faster than the classic predictive model, but, it is a bit slower than the classic model (conventional PI controller). However, this low speed can be ignored due to the advantages of the FMPC in controlling the active and reactive

powers of the wind turbine's converters and damping of the oscillations. In order to verify the effectiveness of the proposed strategy, the eigenvalues for each part of the system are tabulated in Table 2 under different wind speed for the turbines. As seen in this table, the proposed strategy has robust and successful performance in damping oscillations even under different wind speeds, whereas in the conventional method there is the risk of instability without using the predictive controllers and compensator devices. This arises from the fact that by increasing or decreasing the wind speed, the imaginary parts of the eigenvalues are increasing (being more stable) and their real parts are constant or decreasing (being less stable). This means that oscillations damping is decreasing (being less stable) and can trigger a system instability problem.

4.2. Ten-machine thirty-nine-bus power system

In this section, Ten-Machine New-England Power System is employed to evaluate the robustness of the proposed method. The detailed data of this system can be found in [53]. For this purpose, two different scenarios based on three-phase short-circuit fault and changes in the system are investigated. The proposed methods for PI, MPC and FMPC in presence of the SSSC-SCESS are compared together in both cases. The single-line diagram of the system is shown in Fig. 11.

4.2.1. Scenario 1: three-phase short circuit fault

In this scenario a wind farm of 36 MVA equipped with SCESS is connected to bus 14. A three phase fault are applied at $t = 2$ s between buses 3 and 4 and cleared after 0.1 s. The speed of the wind farm is also increased from 11 m per second to 12 m per second at $t = 2$ s with step-size of 0.25. The speed deviations of G_{1-5} and G_{2-4} are depicted in Fig. 12(A) and (B), respectively. The much better damping characteristics using FMPC is acquired for the active power of lines 1–39 and 26–28 as shown in Fig. 12 (C) and (D). As seen in Fig. 12(E) and (F), the reactive power of the wind farm and V_{pcc} are effectively controlled through the predictive strategy and has better performance in damping LFOs compared to PI controller. Rotor-side converter switching signals on axis d and q are demonstrated in Fig. 12(G) and (H), respectively. Moreover, the controlled damping signals for SCESS and SSSC using the predictive strategy and PI controller are shown in Fig. 12 (I) and (J), respectively. According to these figures, in addition to improving overshoot and undershoot, the settling time is also significantly decreased using FMPC controller. The average settling time for FMPC, MPC and PI controllers are obtained as 7.112, 11.24 and 19.985, respectively.

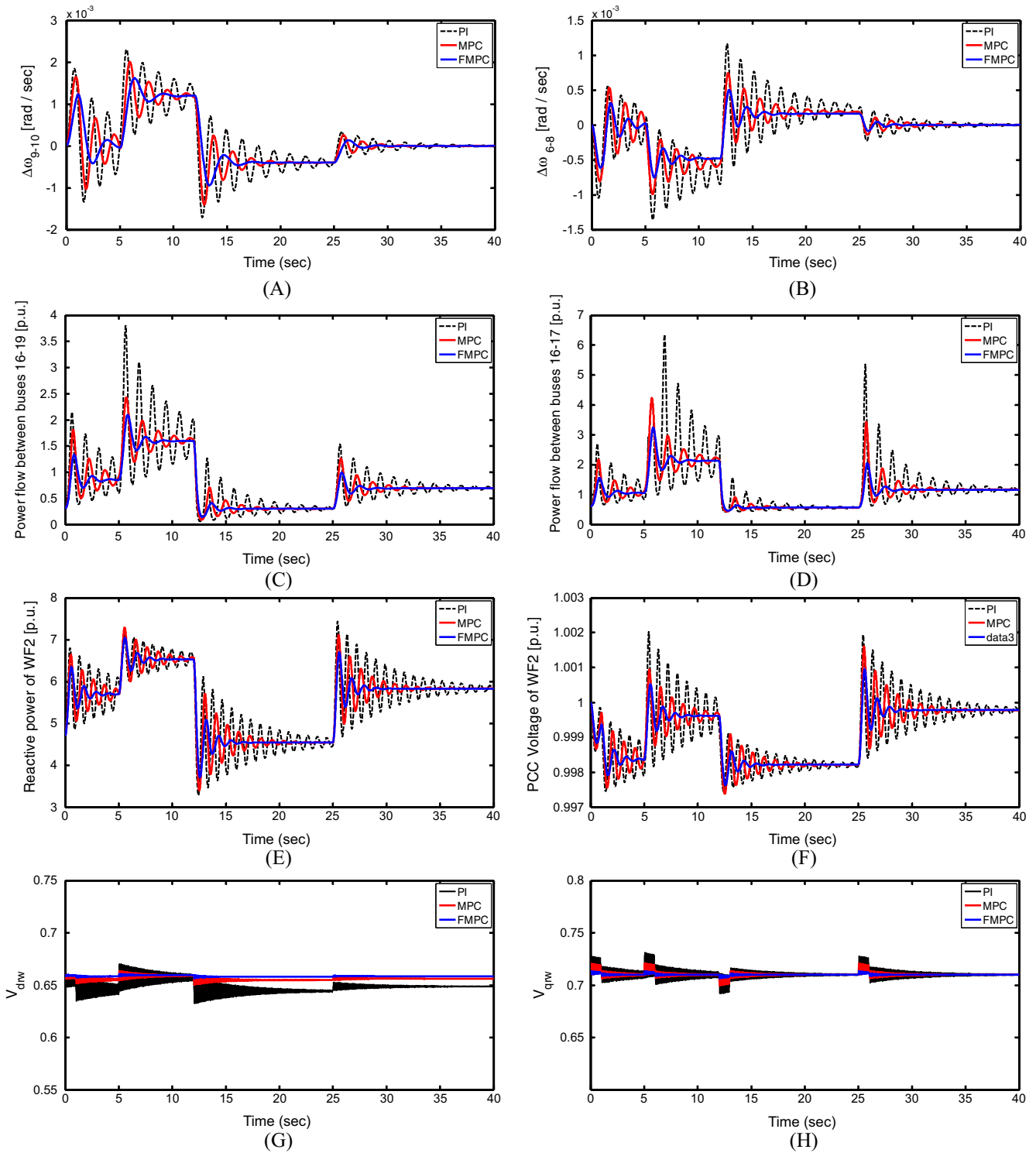


Fig. 14. The response of time-domain simulation of scenario II.

4.2.2. Scenario II: changes in the system load in presence of two wind farms

In this scenario two wind farms with a total rated power output of 72 MVA (36 MVA for each one) connected to buses 14 and 16 are considered. The proposed controller performance under rapid change in load connected to bus 16 is evaluated through following pattern: the load is increased from 3.5 (p.u) to 9.5 (p.u) at $t = 5$ s and then decreased from 9.5 (p.u.) To 1.5 at $t = 12$ s and once again

increased from 1.5 (p.u) to 3.5 (p.u.) at $t = 25$ s. Fig. 13 shows the details of these changes. It should be noted that by increasing the load, the wind speed for both wind turbines is also increased (from 11 m per second to 12 m per second) and decreasing the load results in reducing the wind speed from 12 m per second to 11 m per second. The speed deviations of G_{9-10} and G_{6-8} in terms of the load changes are shown in Fig. 14(A) and (B), respectively. As seen in these figures, the predictive controllers are substantially able to

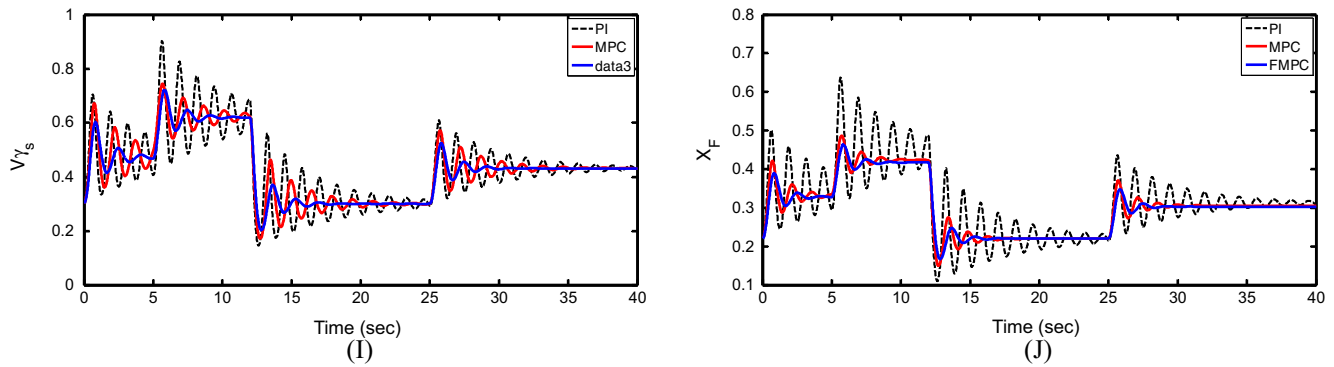


Fig. 14 (continued)

Table 3

The performance of the proposed controllers in terms of objective function and computational time.

Case study	Scenarios	m_a, m_b		Computational time per iteration		Cost function	
		MPC	FMPC	MPC	FMPC	MPC	FMPC
–	–	–	–	–	–	–	–
10 Machine	I	200,80	200,5	4.22	0.46	0.162	0.144
	II	200,80	200,5	5.87	0.51	0.167	0.146
4 Machine	–	200,80	200,5	4.11	0.41	0.158	0.134

respond to the load changes and mitigate the resultant deviations. The active power variations of lines 16–19 and 16–17 are shown in Fig. 14(C) and (D), respectively. As seen in these figures, by decreasing the load at $t = 5$ s, the power flow between lines is initially increased and then by increasing the load at $t = 12$ s the power is declined. Finally, decreasing the load at $t = 25$ s results in increasing the power flow between lines. The reactive power variations and V_{pcc} related to the second wind farm are depicted in Fig. 14(E) and (F), respectively. Fig. 12(G) and (H) respectively shows rotor-side converter switching signals on axis d and q. Furthermore, the input damping signals for SCESS and SSSC through the predictive controllers and PI controller are illustrated in Fig. 14(I) and (J), respectively. According to obtain results from this scenario, the robustness of the predictive controllers is confirmed under rapid power changes compared to PI controller and it is also verified that FMPC has much effective ability in damping oscillations in comparison to MPC and PI.

4.3. Computational aspects of the method

In this section the performance of FMPC and MPC controllers in terms of computational time and objective functions are evaluated. As seen in the table, the value of objective function for FMPC is far less than MPC for both power systems. Since the objective function is defined as the difference between input and output signals, it can be concluded that the least value in this case represents the optimal performance of the controllers. Given that the unknown variables in FMPC are 16 times less than MPC, therefore the computational time for each iteration of FMPC is much less than that of MPC as shown in Table 3. This reduction in the computational time can be considered as a benefit for FMPC controller.

5. Conclusion

In this paper FMPC strategy is proposed as an analytical method to enhance power system stability and is compared with model-based predictive controller and classic controller (without using predictive control). In this technique the Laguerre function is used to reduce computational effort in selecting input paths and also in order to decrease sampling time in the prediction horizon the exponential data weighting is employed. A four-machine and ten-machine power systems are

employed to evaluate the effectiveness of the proposed FMPC scheme. The tested power systems include wind turbines and SCESS and SSSC compensators. The main duty of the SCESS is to control the active power of GSC in the wind turbines. Moreover, SSSC is used to reduce low frequency oscillations through designing a damping controller (using FMPC and MPC methods) for each of the compensators. In addition, the active and reactive power control are carried out on the RSC to acquire appropriate control signals (v_{qrw}, v_{drw}) to improve the power system stability. A three phase fault is applied to both power systems in MATLAB/Simulink environment to run simulations. It is verified through simulation results that the FMPC and MPC strategies have better abilities in damping low frequency oscillations as well as active and reactive power control compared to the conventional method. Furthermore, 20 wind turbines are used in the four-machine power system as a wind farm and the eigenvalues under different wind speeds are extracted and evaluated. The more desirable eigenvalues and consequently better stability enhancement is acquired through the FMPC strategy compared to other Cases.

Appendix A

See Table 1.

References

- [1] Ramasamy M, Thangavel S. Optimal utilization of hybrid wind–solar system as DVR for voltage regulation and energy conservation. *J Circ Syst Comput* 2014;23:1450062.
- [2] Dhanapal S, Anita R. Voltage and frequency control of stand alone self-excited induction generator using photovoltaic system based STATCOM. *J Circ Syst Comput* 2016;25(4):1650031.
- [3] Suvire GO, Mercado PE. Active power control of a flywheel energy storage system for wind energy applications. *IET Renew Power Gener* 2012;6(1):9–16.
- [4] Darabian M, Jalilvand A. PSSs and SVC damping controllers design to mitigate low frequency oscillations problem in a multi-machine power system. *J Electr Eng Technol* 2014;9(4):1873–81.
- [5] Dongkyoung C, Kyo-Beum L. Variable structure control of the active and reactive powers for a DFIG in wind turbines. *IEEE Trans Industr Appl* 2010;46(6).
- [6] Darabian M, Jalilvand A, Noroozian R. The combined use of sensitivity analysis and hybrid wavelet-PSO-ANFIS to improve dynamic performance of DFIG based wind generation. *J Oper Autom Power Eng* 2014;2(1):60–73.
- [7] Bhinal M, Praghnes B, Vivek P. Small signal stability enhancement of DFIG based wind power system using optimized controllers parameters. *Electr Power Energy Syst* 2015;70:70–82.

- [8] Xinze X, Hua MG, Geng Y. Enhanced model of the doubly fed induction generator-based wind farm for small-signal stability studies of weak power system. *IET Renew Power Gener* 2014;8(7):765–74.
- [9] Yang L, Qstergaard Z, Dong ZY, Wong KP. Oscillatory stability and eigenvalue sensitivity analysis of a DFIG wind turbine system. *IEEE Trans Energy Convers* 2011;26(1):328–39.
- [10] Zamaniyar M, Fani B, Golshan MEH, Karshenas HR. Dynamic modeling and optimal control of DFIG wind energy systems using DFT and NSGA-II. *Electr Power Syst Res* 2014;108:50–8.
- [11] Ehsanolah A, Mojtaba. A novel approach to capture the maximum power from variable speed wind turbines using PI controller, RBF neural network and GSA evolutionary algorithm. *Renew Sustain Energy Rev* 2015;51:1023–37.
- [12] Sharon R, Kumudinidevi RP, Bharathidasan SG, Evangelin JV. Coordinated controller design of grid connected DFIG based wind turbine using response surface methodology and NSGA II. *Sust Energy Technol Assessments* 2014;8:120–30.
- [13] Taveiros FEV, Barros LS, Costa FB. Back-to-back converter state-feedback control of DFIG (doubly-fed induction generator)-based wind turbines. *Energy* 2015;89:896–906.
- [14] Tossaporn S, Issarachai N. Robust power oscillation damper design for DFIG-based wind turbine based on specified structure mixed H₂/H_∞ control. *Renew Energy* 2014;66:15–24.
- [15] Mazlumi K, Darabian M, Azari M. Adaptive fuzzy synergetic PSS design to damp power system oscillations. *J Oper Autom Power Eng* 2013;1(1):43–53.
- [16] Jabr HM, Lu D, Kar NC. Design and implementation of neuro-fuzzy vector control for wind-driven doubly-fed induction generator. *IEEE Trans Sust Energy* 2011;2(4):404–13.
- [17] Gkavanoudis SI, Demoulias CS. A combined fault ride-through and power smoothing control method for full-converter wind turbines employing Supercapacitor Energy Storage System. *Electr Power Syst Res* 2014;106:62–72.
- [18] Hasan NS, Hassan MY, Majid MS, Rahman HA. Review of storage schemes for wind energy systems. *Renew Sustain Energy Rev* 2013;21:237–47.
- [19] Iglesias RL, Arantegui RL, Alonso MA. Power electronics evolution in wind turbines a market-based analysis. *Renew Sustain Energy Rev* 2011;15:4982–93.
- [20] Liyan Q, Wei Q. Constant power control of DFIG wind turbines with supercapacitor energy storage. *IEEE Trans Industr Appl* 2011;47(1).
- [21] Farzana I, Ahmed AD, Muyeen SM. Smoothing of wind farm output by prediction and supervisory-control-unit-based FESS. *IEEE Trans Sust Energy* 2013;4(4).
- [22] Xianchao S, Yufei T, Haibo H, Jinyu W. Energy-storage-based low-frequency oscillation damping control using particle swarm optimization and heuristic dynamic programming. *IEEE Trans Power Syst* 2014;29(5).
- [23] Muyeen SM, Hany M, Hasanien B, Ahmed AD. Transient stability enhancement of wind farms connected to a multi-machine power system by using an adaptive ANN-controlled SMES. *Energy Convers Manage* 2014;78:412–20.
- [24] Yong W, Jun Z. Extended backstepping method for single-machine infinite-bus power systems with SMES. *IEEE Trans Control Syst* 2013;21(3).
- [25] Zheng W, Yuwen B, Yongqiang L, Ming C. Improvement of operating performance for the wind farm with a novel CSC-type wind turbine-SMES hybrid system. *IEEE Trans Power Delivery* 2013;28(2).
- [26] Kamel S, Jurado F, Chen Z. Power flow control for transmission networks with implicit modeling of static synchronous series compensator. *Electr Power Energy Syst* 2015;64:911–20.
- [27] Jean DE, Dieu NN, Godpromesse K, René KF, André C, Hilaire BF, et al. A simplified nonlinear controller for transient stability enhancement of multimachine power systems using SSSC device. *Electr Power Energy Syst* 2014;54:650–7.
- [28] Mojtaba A, Soheil G, Morteza A. Wavelet neural adaptive proportional plus conventional integral-derivative controller design of SSSC for transient stability improvement. *Eng Appl Artif Intell* 2013;26:2227–42.
- [29] Bangjun L, Shumin FA. Brand new nonlinear robust control design of SSSC for transient stability and damping improvement of multi-machine power systems via pseudo-generalized Hamiltonian theory. *Control Eng Pract* 2014;29:147–57.
- [30] Rajendra KK, Jitendriya KS. Time delay approach for PSS and SSSC based coordinated controller design using hybrid PSO–GSA algorithm. *Electr Power Energy Syst* 2015;71:262–73.
- [31] Sidhartha P, Narendra KY, Sangram KM. Hybrid BFOA–PSO approach for coordinated design of PSS and SSSC-based controller considering time delays. *Electr Power Energy Syst* 2013;49:221–33.
- [32] Dinh-Nhon T, Van-Thuyen N. Designed damping controller for SSSC to improve stability of a hybrid offshore wind farms considering time delay. *Electr Power Energy Syst* 2015;65:425–31.
- [33] Wang Li, Quang-Son V. Power flow control and stability improvement of connecting an offshore wind farm to a one-machine infinite-bus system using a static synchronous series compensator. *IEEE Trans Sust Energy* 2013;4(2).
- [34] Camponogara E, Scherer HF. Distributed optimization for model predictive control of linear dynamic networks with control-input and output constraints. *IEEE Trans Autom Sci Eng* 2011;8(1):233–42.
- [35] Bijami E, Askari J, Farsangi MM. Design of stabilising signals for power system damping using generalised predictive control optimised by a new hybrid shuffled frog leaping algorithm. *IET Gener Transm Distrib* 2012;6(10):1036–45.
- [36] Darabian M, Jalilvand A, Azari M. Power system stability enhancement in the presence of renewable energy resources and HVDC lines based on predictive control strategy. *Electr Power Energy Syst* 2016;80:363–73.
- [37] Alfeu J, Sgarezi F, Milton E, Oliveira F, Ernesto RF. A predictive power control for wind energy. *IEEE Trans Sust Energy* 2011;2(1).
- [38] Alfeu J, Sgarezi F, Ernesto RO. Model-based predictive control applied to the doubly-fed induction generator direct power control. *IEEE Trans Sust Energy* 2012;3(3).
- [39] Han J, Khushalani S, Solanki J. Coordinated predictive control of a wind/battery microgrid system. *IEEE J Emerg Sel Top Power Electron* 2013;1(4).
- [40] Wang Z, Wang J, Chen B, Begovic MM, He H. MPC-based voltage/var optimization for distribution circuits with distributed generators and exponential load models. *IEEE Trans Smart Grid* 2014;5(5).
- [41] Jun Y, Wei XZ. Offset-free nonlinear MPC for mismatched disturbance attenuation with application to a static var compensator. *IEEE Trans Circ Syst—II: Express Briefs* 2014;61(1).
- [42] Ford JJ, Ledwich G, Dong ZY. Efficient and robust model predictive control for first swing transient stability of power systems using flexible AC transmission systems devices. *IET Gener Transm Distrib* 2008;2(5):731–42.
- [43] Baocang D, Xubin P. Output feedback predictive control with one free control move for nonlinear systems represented by a Takagi-Sugeno model. *IEEE Trans Fuzzy Syst* 2014;22(2).
- [44] Zheng Yi, Shaoyuan L, Ning L. Distributed model predictive control over network information exchange for large-scale systems. *Control Eng Pract* 2011;19:757–69.
- [45] Mincho H, Ventsislav A. Predictive functional control using a blending approach. *Cybernet Informat. Technol* 2005;5(2).
- [46] Huixian L, Shihua L. Speed control for PMSM servo system using predictive functional control and extended state observer. *IEEE Trans Industr Electron* 2012;59(2).
- [47] Anderson PM, Fouad AA. Power system control and stability. Ames (IA, USA): The Iowa State Univ. Press; 1977.
- [48] Zong Yi, Kullmann D, Thavlov A, Gehrke O, Bindner HW. Application of model predictive control for active load management in a distributed power system with high wind penetration. *IEEE Trans Smart Grid* 2012;3:1055–62.
- [49] Evans MA, Mark C, Basil K. Robust MPC tower damping for variable speed wind turbines. *IEEE Trans Control Syst Technol* 2015;23:290–6.
- [50] Wang L. Discrete model predictive control design using Laguerre functions. *J Process Control* 2004;14(2):131–42.
- [51] Valencia-Palomo G, Rossiter JA. Novel programmable logic controller implementation of a predictive controller based on Laguerre functions and multiparametric solutions. *IET Control Theory Appl* 2012;6(8):1003–14.
- [52] Wang L. Use of exponential data weighting in model predictive control design. In: Proc 40th IEEE conference on decision and control. p. 4857–61.
- [53] Pai M. Energy function analysis for power system stability. Berlin (Germany): Springer; 2012.